Statistical analysis of the temporal dynamics of coupling in strongly coupled multi-core fibers

Citation for the original published paper (version of record):

Raj, M., Hayashi, T., Andrekson, P. et al (2026). Statistical analysis of the temporal dynamics of coupling in strongly coupled multi-core fibers. Optics Express, 34(14): 25321-25333.
http://dx.doi.org/10.1364/OE.599061

Research Article | Vol. 34, No. 14 / 13 Jul 2026 / Optics Express 25321

Optics EXPRESS

Statistical analysis of the temporal dynamics of coupling in strongly coupled multi-core fibers

MANISH RAJ,[1,*] TETSUYA HAYASHI,[2] PETER ANDREKSON,[1] AND MAGNUS KARLSSON[1]

[1] *Department of Microtechnology and Nanoscience, Chalmers University of Technology, Kemivägen 9, Gothenburg 41296, Sweden*
[2] *Optical Communications Laboratory, Sumitomo Electric Industries, Ltd., 1, Taya-cho, Sakae-ku, Yokohama 244-8588, Japan*
[*] *manish.raj@chalmers.se*

Abstract: With the growing demand for data traffic, new types of optical fiber have been proposed to address the capacity crisis of existing single-mode fiber infrastructure. Space-division multiplexed (SDM) systems promise to exploit multiple spatial channels for parallel data transmission. The aim of this study is to provide a systematic approach to experimentally investigate the fluctuations of random coupling in the temporal domain of coupled multi-core fibers (MCFs). Understanding these temporal dynamics is crucial to setting requirements for digital signal processing and to developing robust signal recovery algorithms. This is also the first step towards dynamic channel models of these fibers. One of the key requirements for untangling the signals after transmission is accurate knowledge of channel behavior in both the time and frequency domains. We present a statistical and experimental analysis of the temporal dynamics of random coupling in strongly coupled MCFs. Based on a statistical time-drift model, we have experimentally characterized the temporal response of coupled MCFs and their statistical properties, such as the temporal autocorrelation function and the probability density function of fractional optical power.

1. Introduction

With the advent of the internet era, online streaming, video on demand, and millions of simultaneous telephone calls across continents have drastically increased global data consumption [1]. As these vast amounts of data are transmitted through the existing single-mode optical fiber infrastructure, the yearly explosion of data leads to a capacity crisis in conventional optical fiber systems [2–4]. Space-division multiplexing (SDM) is a key technology to address the growing demand for high-capacity optical communications [5–7]. Unlike conventional single-mode single-core fibers, SDM utilizes multiple spatial channels, such as multiple cores or modes, within a single optical fiber to transmit data simultaneously. This approach significantly increases total transmission capacity without requiring a proportional increase in bandwidth [8].

The concept of SDM fibers was introduced as early as 1979 by Inao [9]. However, active research on SDM fibers in recent years has shown the promise of strongly coupled MCFs over other types of optical fibers, such as uncoupled MCFs and weakly coupled MCFs, in many aspects. Multi-core fiber can be divided into two categories based on the nature of coupling between the cores: (1) weakly coupled-core fibers and (2) strongly or randomly coupled-core fibers. In weakly coupled MCFs, the core pitch is large, which results in weak mode coupling between the cores. Whereas strongly (randomly) coupled fibers have some advantages, such as high spatial channel density and low (sublinear) accumulation of differential group delay spread with distance [10]. The presence of strong mode coupling in strongly coupled MCFs gives rise to favorable optical properties, such as the suppression of nonlinear impairments and the reduced accumulation of modal dispersion with distance [11]. However, these fibers

#599061
Journal © 2026
https://doi.org/10.1364/OE.599061
Received 17 Mar 2026; revised 18 May 2026; accepted 9 Jun 2026; published 30 Jun 2026

introduce random mode mixing, which needs to be untangled at the output using multiple-input multiple-output (MIMO) digital signal processing (DSP) [12,13]. The complexity of the MIMO DSP depends on the magnitude of the differential group delay (DGD) spread [14]. However, in such fibers, the random coupling between the cores also introduces inter-core crosstalk and temporal fluctuations in the power distribution. Understanding this dynamic is essential for optimizing fiber and DSP design, improving transmission performance, and mitigating capacity limitations in next-generation optical networks.

The frequency dependence of group delay spreads (GDs) has been studied by Cappelletti et al. [15,16] for field-deployed strongly coupled-core fiber links, where it was shown using the statistical method that random coupling can significantly affect the DGD, an important parameter for optimizing MIMO DSP. A dynamic (time-varying) model of coupling in the same type of fiber was developed by Deriushkina et al. [17] who analyzed both the frequency and time-domain behavior of the DGD and the impulse responses. The authors analytically derived expressions for the frequency and time-domain autocorrelation functions of the fiber.

The analysis of crosstalk in multi-core fibers using statistical and analytical methods has been studied by Ng et al., [18]. They showed that crosstalk in weakly coupled multi-core fibers follows a χ^2 distribution with four degrees of freedom due to random perturbations such as bends, twists, and core diameter variations, which modulate coupling coefficients and phase mismatch. Using coupled mode theory, a closed-form expression for the average crosstalk and its statistical distribution were derived, which helps to estimate the effects of crosstalk on systems. The key factors are core pitch, core geometry, fiber bends and twists, and the correlation length over which perturbations are correlated, all of which govern the statistical behavior of inter-core coupling. In [19], Koshiba et al. presented an analytical expression for the average inter-core crosstalk in weakly coupled seven-core fibers. The study revealed that the average power coupling coefficient (PCC) depends on the bending radius, correlation length, and differences in core propagation constants. For large bending radii and correlation lengths, the PCC scales inversely with the correlation length and with the square of the propagation constant difference; for small bending radii and large correlation lengths, the PCC scales with the bending radius and is independent of the correlation length; and for small correlation lengths, the PCC scales with the correlation length and is independent of the bending radius.

While many of these studies are theoretical and based on numerical modeling, mainly focusing on the frequency dependence of the transfer matrix to study group delays and the intensity impulse response of the optical fiber. Others studied the characterization of crosstalk and the effects of bending and twisting on inter-core crosstalk in weakly coupled MCFs, but very few studies have been reported on experimental investigations of time dynamics of coupling in strongly coupled MCFs. There is limited literature that has experimentally studied the temporal dynamics of optical power fluctuations in strongly coupled MCFs, which arise mainly from environmental perturbations such as acoustic vibrations and surrounding temperature variations. The analysis of the temporal fluctuations of optical power is important for understanding channel properties relevant to data transmission.

In this paper, we experimentally characterize the temporal dynamics of random coupling and use statistical analysis to study the important characteristics of temporal power fluctuations in strongly coupled MCFs. The study of the temporal autocorrelation function and the probability density functions of coupled optical power can give insights into the fundamental behavior of these fibers. The aim of this study is to understand the coupling dynamics in strongly coupled MCFs, which will help to design better channel models and potentially improved SDM systems with appropriate transmission properties.

The article is organized as follows. In Section 2, we describe the mode coupling in an ideal coupled MCF using the supermode picture. The nature and origin of random mode coupling and its effects on power transfer in coupled MCF are discussed. We also present the time dynamics

Optics EXPRESS

model for random coupling. Throughout this paper, we use coupled MCF to emphasize strongly (randomly) coupled multi-core fiber. In Section 3, we explain the experimental procedure and the properties of the coupled MCF used in the experiment. Section 4 discusses the results for the temporal dynamics of random coupling in a coupled MCF and the statistical properties of random coupling, such as the probability density function for temporal fluctuations and the autocorrelation function. Finally, Section 5 presents the conclusion.

2. Theoretical background

In this section, we start with the supermode picture of mode coupling in ideal coupled MCFs. Following this discussion, we discuss the nature of random mode coupling, its origin, and the coupling dynamics in strongly coupled MCFs. The last part of this section presents a temporal dynamics model based on the transfer-matrix method.

2.1. Mode coupling in ideal coupled multi-core fibers

The power coupling in coupled MCFs can be described through supermode analysis. The modal structure of a coupled waveguide system can be represented in terms of supermodes, which are linear combinations of the local modes supported by the individual cores. These supermodes describe the collective field distribution of the entire coupled structure and propagate with well-defined propagation constants [20–22]. In an ideal coupled waveguide, these supermodes correspond exactly to the eigenmodes of the system and are therefore mutually orthogonal and propagate independently without power exchange. As an example, consider a systematically coupled MCF comprising two identical cores. When optical power is launched into the local mode of a single core, the power exhibits a periodic, sinusoidal transfer between the two cores as a consequence of deterministic inter-core coupling. In the supermode representation, however, this excitation is equivalently described as the simultaneous excitation of the two eigenmodes, namely the even and odd supermodes. These eigenmodes propagate independently with distinct propagation constants, and the observed oscillatory power exchange between the cores arises from the coherent beating between them, rather than from coupling between the eigenmodes themselves. Phase matching is related to the difference in propagation constants between supermodes $\Delta\beta$, and the coupling period is given by $1/\Delta\beta$. Phase matching means that this difference is made small. When the supermodes are phase matched, the power transfers efficiently between the cores, and when the propagation constants are far from each other (mismatched), less power is coupled between the cores. For an N-core fiber, the number of supermodes is N.

Mathematically, the propagation of optical fields in a three coupled-core fiber (3CCF) can be described using coupled-mode theory. Let the electric field amplitudes in the equally and symmetrically spaced three coupled-cores be represented by the vector

$$\mathbf{A}(z) = (A_1(z), A_2(z), A_3(z))^T \, . \tag{1}$$

Where A_k denote the complex amplitude of the wave in the core k. The coupled-mode equations can be written as [23]

$$\frac{d\mathbf{A}}{dz} = iM\mathbf{A}, \tag{2}$$

For the scalar model with three coupled-cores [24], the 3×3 coupling matrix $\mathbf{M}$, which captures all mode mixing and coupling dynamics of the coupled MCF, is given by

$$M = \begin{pmatrix} \beta_0 & C & C \\ C & \beta_0 & C \\ C & C & \beta_0 \end{pmatrix}. \tag{3}$$

where β_0 is the propagation constant of an isolated core and C is the coupling coefficient between the cores. The supermodes of the three coupled-core fiber are obtained by solving the eigenvalue problem

$$(\mathbf{M} - \beta \mathbf{I})\, \mathbf{v} = 0, \tag{4}$$

The resulting eigenvalues and eigenvectors corresponding to the supermode propagation constants are given by

$$\begin{aligned} \beta_1 &= \beta_0 + 2C, & \mathbf{v_1} &= \frac{1}{\sqrt{3}}(1, 1, 1) \\ \beta_2 &= \beta_0 - C, & \mathbf{v_2} &= \frac{1}{\sqrt{2}}(1, -1, 0) \\ \beta_3 &= \beta_0 - C, & \mathbf{v_3} &= \frac{1}{\sqrt{6}}(1, 1, -2). \end{aligned} \tag{5}$$

These eigenvalues correspond to one symmetric supermode and two degenerate antisymmetric supermodes. The eigenstates for the 3CCF can be visualized as shown in Fig. 1.

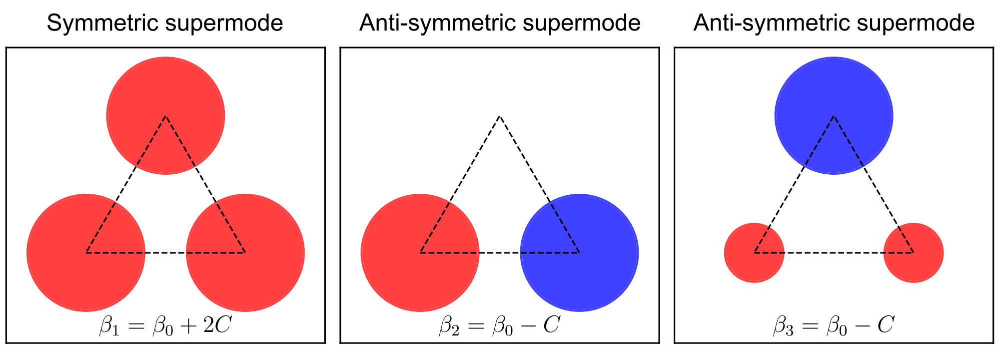

Fig. 1. Schematic representation of the supermodes of a three coupled-core fiber. The symmetric supermode with equal in-phase amplitudes in all cores (left), and two degenerate antisymmetric supermodes with distinct phase and amplitude distributions. Circle size indicates relative field amplitude, and color denotes relative phase.

2.2. Random mode coupling in coupled multi-core fibers

Unlike the ideal coupled MCF, a real multi-core fiber exhibits random coupling in both frequency and time, which comes from both environmental perturbations and fabrication imperfections. The environmental perturbations are due to surrounding temperature variations, acoustic vibrations, bending and twisting of optical fibers, and mechanical stress and strain, which can be caused by macro or micro-bendings. These intrinsic and environmental perturbations degrade the performance of optical fibers and can lead to changes in the physical and optical properties of optical fibers, such as refractive index, phase, state of polarization (SOP) [25] and signal attenuation. The fabrication imperfections are mainly due to variations in core diameter, core asymmetry, core eccentricity, variation in core pitch along the fiber length, and non-uniformity of refractive index. Non-uniform stress during the drawing process of the fiber can also affect the optical properties. These structural imperfections can also induce random birefringence and cause polarization crosstalk.

Efficient power transfer occurs only when the cores are phase matched. The imperfections present in these fibers can lead to inefficient coupling due to phase mismatch between the cores. The random nature of these imperfections causes randomness of coupling in coupled-core optical fibers, which in turn can lead to polarization mode dispersion, as well as differential group delay

[26]. These imperfections also lead to the group-delay mismatch between the supermodes of the coupled structures [27], which usually dominates the impulse response.

The optical fiber that we used in the experiment has strong coupling, which causes the power to be approximately equally distributed among all three cores at the output of the fiber. The frequency dependence of coupling coefficients arises from the intrinsic nature of the refractive index, which is frequency dependent [24]. At higher frequencies, the mode area decreases, which decreases the modal overlap integrals; as a result, the coupling decreases linearly with frequency, as shown in [28] for weakly coupled MCF. The frequency dependence of the coupling exhibits fluctuations on the order of GHz in some fiber installations as reported in [15]. The time-dependent coupling is the result of environmental perturbations (e.g., thermal fluctuations, mechanical and acoustic variations etc.). The coupling exhibits fluctuations in the order of seconds.

2.3. Modeling the temporal dynamics of random coupling

The temporal dynamics of coupling is modeled by the time evolution of a unitary transfer matrix. Most optical fibers have very little mode-dependent loss, which mathematically means that this matrix is unitary. The time dynamics of the optical power can be modeled using a scalar model, and the linear optical response of the coupled multi-core fiber is fully described by a frequency and time-dependent transfer matrix as

$$\mathbf{u}_{\text{out}}(\omega,t) = \mathbf{T}(\omega,t)\mathbf{u}_{\text{in}}, \qquad \mathbf{T}(\omega,t) \in \mathbb{C}^{3\times 3}. \tag{6}$$

where

$$\mathbf{T}(\omega,t) = \begin{pmatrix} m_{11} & m_{12} & m_{13} \\ m_{21} & m_{22} & m_{23} \\ m_{31} & m_{32} & m_{33} \end{pmatrix}. \tag{7}$$

Each matrix element $m_{ij}(\omega,t)$ is a complex number which describes the field transfer from input core j to output core i. The magnitudes of the matrix elements describe propagation loss as well as inter-core coupling effects, while the phases account for the accumulated propagation phase arising from both coupling and environmental factors. The diagonal elements m_{ii} represent field transmission within the same core, whereas the off-diagonal elements m_{ij} $(i \neq j)$ quantify inter-core coupling effects.

The frequency-dependent static random coupling model is discussed in [24,27]. The reader is referred to these references for further details. The propagation of the optical field in a coupled MCF can be modeled by a concatenation rule from the polarization mode dispersion (PMD) formalism. Each segment of length L_d of an ideal coupled MCF is described by a delay matrix $\mathbf{T}_d$. Since the coupling coefficients and birefringence depend on frequency, the coupling matrix becomes frequency dependent [24], and consequently so does the delay matrix $\mathbf{T}_d(\omega)$.

The explicit time dependence of the transfer matrix $T(\omega,t)$ arises from random perturbations along the optical fiber, as discussed above. These perturbations induce temporal variations in the effective propagation constants and coupling coefficients. As a result, even under stationary input excitation, the output fields evolve in time due to the change of both the amplitudes and phases of the transfer matrix elements. Under the assumption of strong mode mixing and statistical isotropy, the real and imaginary parts of the matrix elements can be assumed to be approximately Gaussian random variables with zero mean.

The random coupling in a coupled MCF can be described using a concatenation model, as shown in Fig. 2. In this approach, the fiber is divided into multiple short segments. Between successive segments, random and time-varying unitary coupling matrices U_n are introduced to model environmental perturbations such as temperature fluctuations and mechanical stress.

Optics EXPRESS

Random perturbations in the coupled MCF are introduced through statistically independent unitary perturbations to describe the temporal evolution. These unitary transfer matrices vary with time, and the instantaneous matrix is given by

$$\mathbf{U}(t_{i+1}) = \Delta\mathbf{U}_i \cdot \mathbf{U}(t_i). \tag{8}$$

The time is discretized into small time steps of δt which is the time period between $U(t_i)$ and $U(t_{i+1})$ and each incremental matrix $\Delta\mathbf{U}_i$ models weak environmental fluctuations over one time step and is given by

$$\Delta\mathbf{U}_i = \exp(j\gamma\mathbf{H}_i)\,, \tag{9}$$

where the parameter $\gamma \ll 1$ determines the strength of fluctuations and thereby controls the temporal correlation between consecutive matrices $\mathbf{U}(t_i)$ and $\mathbf{U}(t_{i+1})$. A larger γ leads to stronger fluctuations. A random Hermitian matrix $\mathbf{H}_i = \mathbf{H}_i^{\dagger}$ is chosen from the Gaussian unitary ensemble [17]. The matrices $\mathbf{H}_i$ are assumed to be independent and identically distributed with expectation values

$$\langle \mathbf{H}_i \rangle = 0, \qquad \langle \mathbf{H}_i^2 \rangle = D\,\mathbf{I}, \tag{10}$$

where D is the dimension of the fiber which ensures a statistically isotropic process on the unitary group. After N time steps, the transfer matrix can be expressed as

$$\mathbf{U}(t_N) = \prod_{k=0}^{N-1} \exp(j\gamma\mathbf{H}_k)\,\mathbf{U}(0), \tag{11}$$

which shows that the temporal fluctuations results from the cumulative effects of many weak, independent perturbations. Instead of using a single unitary random matrix U_n for each fiber segment, a set of matrices $U_n(t)$ is introduced at each concatenation step n to obtain the total transfer matrix as done in [17]. The temporal autocorrelation function is discussed in Section 4.3 based on the model presented here.

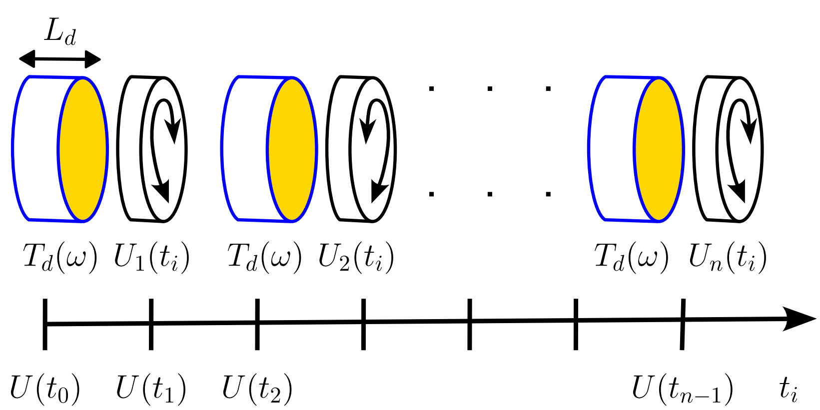

Fig. 2. Time-drift dynamic model for random coupling using a concatenated fiber representation.

3. Experimental description

In this section, we describe the experimental setup used to measure the time fluctuations of random coupling in optical power. The measurements are carried out for the temporal optical power fluctuations with the setup described below. The optical time-domain reflectometer (OTDR) measurements are performed separately for each core using an OTDR device.

Optics EXPRESS

3.1. Experimental setup

The experimental setup shown in Fig. 3 consists of a tunable laser source (Santec TSL-570). The input state of polarization is aligned using a polarization controller (PC) before launching into one of the cores of the coupled MCF. The output of the coupled MCF is measured simultaneously for all cores using New Focus Model 1811 low-noise photoreceivers, which have a bandwidth of 125 MHz and a transimpedance of 40 V/mA. The detected optical signals are recorded using a Tektronix DSA 71604 oscilloscope (OSC) with a temporal resolution of 10 ms. The temporal drift of optical power is recorded under a launch condition with single-mode excitation in each core by launching power into one core at a time for each measurement. Tabletop measurements are performed on a spooled three coupled-core fiber in a general laboratory environment. The optical setup is taped down for mechanical stability. We repeated the measurements over three different days, with a total measurement time of 150 minutes, to obtain reliable statistical data for analyzing the temporal dynamics of the coupling. The back-to-back experimental setup with the laser source and detector has an SNR of about 34 dB, and the optical setup is mainly limited by thermal noise. The laser source is quite stable, with a RIN of about −145 dB/Hz. The loss profile of each core in the coupled MCF is measured using the OTDR technique, as shown in Fig. 4. The OTDR traces for all three cores have nearly identical slopes, which indicate the same attenuation in each core. The observed vertical offset, as shown in Fig. 4 inset, is mainly attributed to splice loss and insertion loss of the fan-in/fan-out device, which are not identical for all three cores.

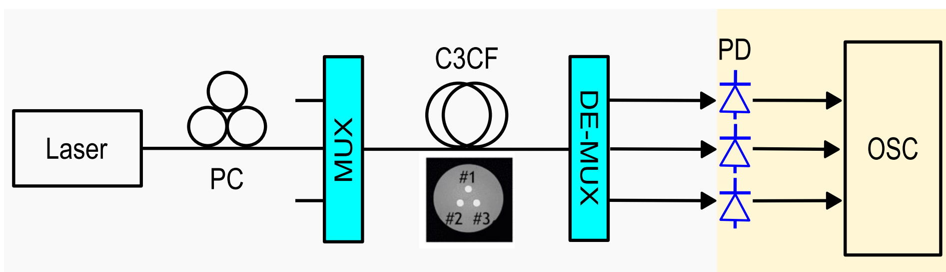

Fig. 3. Schematic of the experimental setup for measuring temporal fluctuation of optical power over time. The inset shows the cross section of the 3CCF.

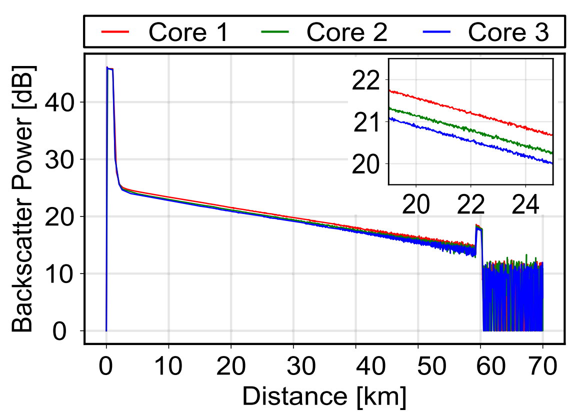

Fig. 4. The OTDR traces for all three cores are shown. The inset shows a zoomed-in view of the separation between the traces for the individual cores.

Optics EXPRESS

The coupled MCF used in this paper has a total length of 59.3 km. The fiber is a three coupled-core fiber with equidistant cores that lie on an equilateral triangle. The distance from the center to each of the cores is 17 µm, which results in a core pitch of 29.4 µm. The cladding diameter is 125 µm, as in a standard SMF fiber. The core diameter is 12.4 µm, and the refractive index difference is 0.27%. When light is launched at 1550 nm into one of the cores and the output is measured from all the cores, the attenuation of the light is 0.181 dB/km. The difference from the total loss can be attributed to connector and splice losses, as well as the insertion loss of the Fan-In/Fan-Out device. The fiber is designed with a cutoff wavelength around 1340–1360 nm for a single core. The chromatic dispersion and dispersion slope of the fiber at 1550 nm correspond to 21 ps/(nm · km) and 0.06 ps/(nm^2 · km), respectively. This fiber was also used in various transmission experiments performed in [14,29].

4. Statistical properties of random coupling in temporal domain

In this section, we present experimental results on the temporal fluctuations of random coupling in coupled MCF. The key statistical properties of the coupled power, such as statistical moments, temporal autocorrelation, and statistical distribution functions, are described below.

Consider a symmetric three coupled-core fiber, where each core supports two orthogonal polarization modes. The optical field in the system can be described by the complex amplitudes of the transfer matrix elements, m_{ij}. If only one core is excited, the input field is $\mathbf{u}_{\text{in}} = u_0(1, 0, 0)^{\text{T}}$, and the corresponding output field is given by

$$\mathbf{u}_{\text{out}}(\omega, t) = \mathbf{T}(\omega, t)\,\mathbf{u}_{\text{in}} = u_0 \begin{pmatrix} m_{11}(\omega, t) \\ m_{21}(\omega, t) \\ m_{31}(\omega, t) \end{pmatrix}. \tag{12}$$

The total output power is defined as the squared Euclidean norm of the output field vector,

$$P_{\text{tot}}(t) = |\mathbf{u}_{\text{out}}(\omega, t)|^2 = \mathbf{u}^{\dagger}_{\text{out}}(\omega, t)\mathbf{u}_{\text{out}}(\omega, t). \tag{13}$$

Substituting the above expression gives the total optical power,

$$P_{\text{tot}}(t) = |u_0|^2 \begin{pmatrix} m^*_{11} & m^*_{21} & m^*_{31} \end{pmatrix} \begin{pmatrix} m_{11} \\ m_{21} \\ m_{31} \end{pmatrix} = |u_0|^2 \sum_{i=1}^{3} |m_{i1}(\omega, t)|^2 = |u_0|^2 \tag{14}$$

which is conserved (independent of time and frequency). In general, the total output power can also be written as

$$P_{\text{tot}}(t) = \mathbf{u}^{\dagger}_{\text{in}}\mathbf{T}^{\dagger}(\omega, t)\mathbf{T}(\omega, t)\mathbf{u}_{\text{in}} = \mathbf{u}^{\dagger}_{\text{in}}\mathbf{u}_{\text{in}} \tag{15}$$

thanks to the unitary nature of $\mathbf{T}$. The optical power at the output of core i is given by

$$P_i(t) = \left| \sum_{j=1}^{3} m_{ij}(\omega, t)\, u^{\text{in}}_j \right|^2. \tag{16}$$

where u^{in}_j denotes the input optical field. The temporal fluctuations of the matrix elements directly translate into measurable power fluctuations through interference among multiple coupling paths.

4.1. Barycentric coordinate representation

By introducing the normalized power fractions $p_i = P_i(t)/P_{\text{tot}}$, the constraint $p_1 + p_2 + p_3 = 1$ is satisfied, and the state of the system is fully specified by the triplet (p_1, p_2, p_3). The instantaneous power between the three cores mixes in a random fashion, but the powers in all three cores remain correlated, since only a fraction of the total power is coupled into each core. The fractional powers (p_1, p_2, p_3) can be represented by barycentric coordinates within a two dimensional simplex (triangle), which provides a convenient geometric representation of the power sharing among the three cores [30]. This geometric representation provides an intuitive visualization of the stochastic power distribution among the cores as shown in Fig. 5(b). Lines parallel to a side of the triangle correspond to a constant fractional power, p_i = constant, while a line passing through a vertex represents the relative power ratio between the cores. The triplet (p_1, p_2, p_3) can be mapped to a two-dimensional simplex using

$$x = p_2 + \frac{1}{2}p_3, \qquad y = \frac{\sqrt{3}}{2}p_3. \tag{17}$$

Here, x and y are the Cartesian coordinates of the point in the triangle, with x representing the contributions of cores 2 and 3, and y representing the contribution of core 3. The fractional power in core 1, $p_1 = 1 - p_2 - p_3$, is implicit, as its vertex is at the origin.

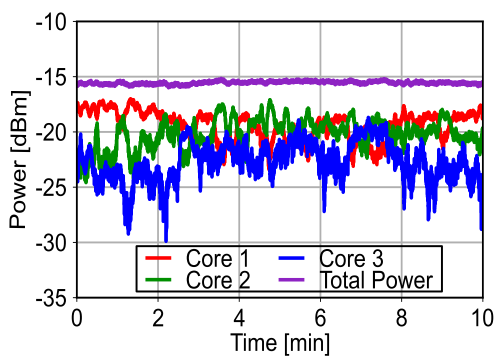

(a)

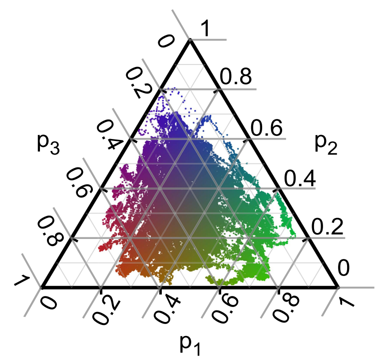

(b)

Fig. 5. Figure showing (a) the measured temporal fluctuations of instantaneous coupled optical power in a strongly coupled MCF (b) and its 2D simplex representation. The center lobe shows that the power is equally distributed among the cores.

The vertices correspond to complete power localization in a single core, the edges represent power exchange between two cores, and the interior points indicate simultaneous power distribution among three cores. The simplex representation shows that the probability density is maximal near the center of the triangle, corresponding to near-equipartition of power, and decreases toward the corners, reflecting a reduced likelihood of strong power localization. To determine the fractional powers from the simplex plot, one can use the perpendicular distance from the point of interest to each of the three sides of the triangle. The distances, or their ratios relative to the triangle height, directly give the values of p_1, p_2, and p_3. Figure 5(b) shows the two dimensional simplex representation of the fractional coupled power. The probability density is concentrated near the center, indicating a high likelihood that the optical power is distributed nearly equally among all three cores. The displacement from the center toward a side or vertex of the triangle reflects skewness toward the dominance of one core over the others. The instantaneous optical power mixing among the cores over time is shown in Fig. 5(a). The optical power for each core, as well as the total power, is unnormalized and corresponds to the actual recorded power over time. For

Optics EXPRESS

an input optical power of 1 mW launched into one core, the mean optical power is about 0.01 mW with a standard deviation of about 0.00504 mW per core. Although the optical power in each core fluctuates in time due to random inter-core coupling, the total instantaneous power remains nearly constant, as seen in Fig. 5(a). The optical power is redistributed among the cores as a result of strong inter-core coupling. Fluctuations in the total optical power arises from unequal losses in the fan-in and fan-out (FIFO) couplers and splices with the FIFO. Other possible reasons include slightly different attenuation coefficients of the three cores (as evident from the OTDR traces shown in Fig. 4), leakage from the cores to the cladding or radiation modes, mode-dependent loss, and measurement noise of the detector. These fluctuations are small compared to the individual core fluctuations and can be considered approximately constant over time.

4.2. Probability density function of optical power fluctuations

The random perturbation in coupled-core fiber can be introduced by a random unitary matrix in the transfer matrix for the coupled modes between the successive concatenations as explained in Section 2. Such a unitary matrix is statistically described by the Haar distribution [31], which ensures power conservation and statistically isotropic mode mixing. Due to power conservation, the squared magnitudes of the matrix elements in each row of the transfer matrix form a normalized set of non-negative random variables whose sum equals unity. Such vectors lie on a simplex and can be modeled by the multivariate Dirichlet distribution [32]. The fractional power at the output of a single core corresponds to the marginal distribution of one component of this Dirichlet distribution, which yields a Beta distribution. The fraction of optical power in each core, when normalized by the total power, follows a Beta distribution. The Beta distribution derived from the 3-variate Dirichlet distribution is given as [33]

$$\mathcal{P}(p;\alpha) = \frac{1}{B\,(\alpha)} \cdot p^{\alpha-1}(1-p)^{2\alpha-1}, \quad 0<p<1,\ \alpha>0 \tag{18}$$

The normalization constant $B(\alpha)$ guarantees that the total probability integrates to one. It is given by

$$B(\alpha) = \frac{\Gamma(\alpha)\,\Gamma(2\alpha)}{\Gamma(3\alpha)}. \tag{19}$$

Where Γ denotes the gamma function, and α is the only free parameter that controls the spread and uniformity of the distribution. Physically, it is related to the variance (spread) of normalized power. To illustrate the effect of α, we consider two cases with $\alpha = 2$ and $\alpha = 6$, as shown in Fig. 6(a) and (b). This allows us to compare the distribution of normalized power across the three components for different values of α. As shown in Fig. 6(a), the distribution is more uniform and the lobe is spread out from the center, whereas in Fig. 6(b) it becomes more concentrated towards the center. $\alpha = 1$ corresponds to a uniform distribution, while higher values of α lead to more peaked distributions. In this sense, α controls the statistical distribution of power among modes, as well as the strength of fluctuations in the normalized modal power distribution. In our case, the analytical fit to measurements gives $\alpha = 3.05$ as shown in Fig. 7(a). The mean and variance of the Beta distribution are given by [34]

$$\mathbb{E}[p] = \frac{1}{3}, \quad \mathrm{Var}[p] = \frac{2}{9(3\alpha+1)} \tag{20}$$

Based on the values of α obtained from the analytical fit, the mean and variance are 0.33 and 0.022, respectively. For symmetric cores with identical statistical properties, the power is expected to be equally distributed among the three cores, corresponding to a mean power of 0.33 per core, which indeed agrees with the measured value.

The Beta distribution arises from the higher probability of low-power states, resulting from the cumulative effects of random phase drifts and inter-core coupling in concatenated fiber

Optics EXPRESS

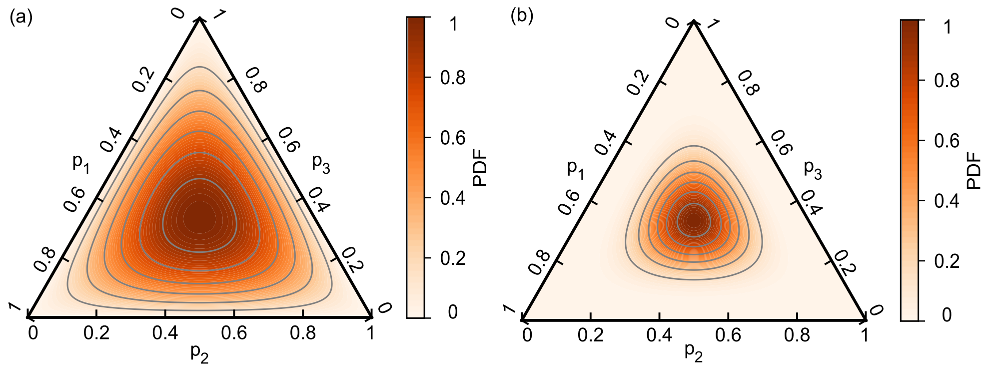

Fig. 6. Illustrative examples of the Dirichlet distribution for the normalized power in the symmetric case with (a) $\alpha = 2$ and (b) $\alpha = 6$.

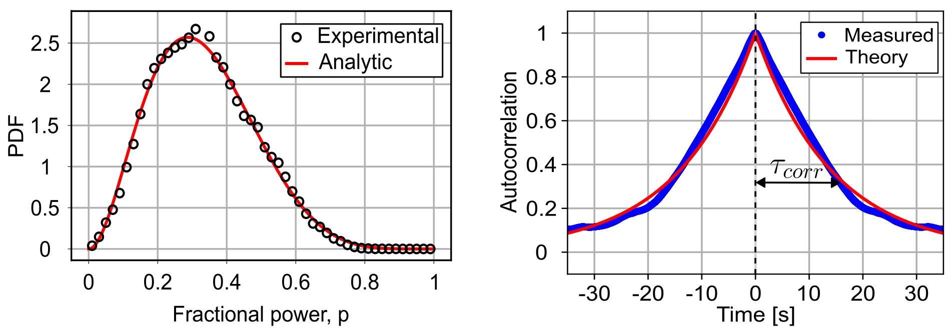

(a) (b)

Fig. 7. Figure showing (a) the probability density function (PDF) of the measured optical power fluctuations, which is well fitted by the beta distribution (red), and (b) the corresponding temporal autocorrelation function.

segments. Phase variations predominantly induce partial destructive interference, reducing power in a given mode, while weak or asymmetric coupling allows only partial energy transfer, which further favor the lower power levels. As light propagates through multiple segments, these effects accumulate, producing a distribution in which low-power states are more frequent. Figure 7(a) shows the measured PDF of normalized powers averaged across all cores along with the theoretical distribution.

4.3. Autocorrelation function

Based on the model described in section 2.3, the temporal autocorrelation function (ACF) of the channel is defined as

$$R_{tt'} = \frac{1}{D}\,\mathrm{Tr}\left\langle \mathbf{U}^{\dagger}(t')\mathbf{U}(t)\right\rangle, \tag{21}$$

Here, D is the dimension of the transfer matrix, and the analytical expression for the ACF can be given by

$$R_{tt'} = \exp\left(-\frac{|t-t'|}{\tau_{\mathrm{corr}}}\right). \tag{22}$$

For the analysis of the ACF, we averaged the ACF of each core across data sets collected on different measurement days. The temporal autocorrelation function is shown in Fig. 7(b). The

Optics EXPRESS

correlation width is defined as the separation τ_{corr} at which the normalized autocorrelation falls to $1/e$ of its peak value. The width of the autocorrelation is about 17 s. It provides a characteristic time scale on which the signal remains correlated with itself [35]. The ACF decays exponentially with the characteristic correlation time τ_{corr}. The origin of these fluctuations is mainly due to environmental perturbations, as discussed in Section 2.2. The correlation time physically captures the typical time over which external perturbations, such as temperature variations, mechanical vibrations, or other environmental drifts, cause the system to decorrelate. In other words, a small τ_{corr} corresponds to rapid decorrelation due to fast environmental fluctuations, whereas a large τ_{corr} indicates slow decorrelation, with the system remaining correlated for longer times.

5. Conclusions

In this work, we have presented a theoretical and experimental study of the temporal dynamics of random coupling in spooled strongly coupled multi-core fibers under laboratory environments. By analyzing the statistical characteristics of coupled MCF, we have shown that the statistical distributions of the fractional optical power per core follow a beta distribution. Using a time-drift model, we analyzed the temporal response of the random coupling and investigated its autocorrelation and probability density function in the linear propagation regime. The results provide important insights into the time-varying nature of random coupling in coupled MCFs. This study is based on measurements from a spooled three coupled-core fiber under laboratory conditions, which may differ from the statistics observed in field-deployed MCFs due to environmental perturbations affecting the fibers differently. Understanding the temporal dynamics is crucial to assess their impact on MIMO DSP and to develop robust signal recovery algorithms. Furthermore, the analysis presented here can provide useful insights for the design, optimization, and performance evaluation of space-division multiplexing transmission systems and sensing devices based on coupled MCFs.

Funding. Horizon Europe – Marie Skłodowska-Curie Doctoral Network HOMTech (101072409); Swedish Research Council (Vetenskapsrådet, VR) (2025-0384).

Acknowledgment. The authors would like to thank Ekaterina Deriushkina for discussions on the dynamic coupling model and for providing valuable insights for this work. We also would like to thank Mikael Mazur for lending us the fiber, and for many helpful discussions.

Disclosures. The authors declare no conflicts of interest related to this article.

Data availability. Data underlying the results presented in this paper are available in Ref [36].

References

1. D. J. Richardson, J. M. Fini, and L. E. Nelson, "Space-division multiplexing in optical fibres," Nat. Photonics **7**(5), 354–362 (2013).
2. R.-J. Essiambre, G. Kramer, P. J. Winzer, *et al.*, "Capacity limits of optical fiber networks," J. Lightwave Technol. **28**(4), 662–701 (2010).
3. R.-J. Essiambre and R. W. Tkach, "Capacity trends and limits of optical communication networks," Proc. IEEE **100**(5), 1035–1055 (2012).
4. A. Ellis, N. M. Suibhne, D. Saad, *et al.*, "Communication networks beyond the capacity crunch," Phil. Trans. R. Soc. A. **374**(2062), 20150191 (2016).
5. G. Li, N. Bai, N. Zhao, *et al.*, "Space-division multiplexing: the next frontier in optical communication," Adv. Opt. Photonics **6**(4), 413–487 (2014).
6. T. Mizuno and Y. Miyamoto, "High-capacity dense space division multiplexing transmission," Opt. Fiber Technol. **35**, 108–117 (2017).
7. S. Chandrasekhar, A. Gnauck, X. Liu, *et al.*, "Wdm/sdm transmission of 10× 128-gb/s pdm-qpsk over 2688-km 7-core fiber with a per-fiber net aggregate spectral-efficiency distance product of 40,320 km· b/s/hz," in *European Conference and Exposition on Optical Communications*, (Optica Publishing Group, 2011), pp. Th–13.
8. B. J. Puttnam, G. Rademacher, and R. S. Luís, "Space-division multiplexing for optical fiber communications," Optica **8**(9), 1186–1203 (2021).
9. S. Inao, "High density multi-core-fiber cable," in *Proc. of the 28th International Wire & Cable Symposium (IWCS), 1979*, (1979), pp. 370–384.

10. R. Ryf, S. Randel, A. H. Gnauck, *et al.*, "Mode-division multiplexing over 96 km of few-mode fiber using coherent 6× 6 mimo processing," J. Lightwave Technol. **30**(4), 521–531 (2012).
11. T. Hayashi, T. Sakamoto, Y. Yamada, *et al.*, "Randomly-coupled multi-core fiber technology," Proc. IEEE **110**(11), 1786–1803 (2022).
12. K. Shibahara, T. Mizuno, D. Lee, *et al.*, "Advanced mimo signal processing techniques enabling long-haul dense sdm transmissions," J. Lightwave Technol. **36**(2), 336–348 (2017).
13. S. Beppu, K. Igarashi, M. Kikuta, *et al.*, "Real-time mimo-dsp technologies for sdm systems," in *2021 Optical Fiber Communications Conference and Exhibition (OFC)*, (IEEE, 2021), pp. 1–3.
14. R. Ryf, R.-J. Essiambre, A. Gnauck, *et al.*, "Space-division multiplexed transmission over 4200-km 3-core microstructured fiber," in *National Fiber Optic Engineers Conference*, (Optica Publishing Group, 2012), pp. PDP5C–2.
15. M. Cappelletti, M. Mazur, N. K. Fontaine, *et al.*, "Statistical analysis of modal dispersion in field-installed coupled-core fiber link," J. Lightwave Technol. **42**(11), 4103–4109 (2024).
16. M. Mazur, N. K. Fontaine, R. Ryf, *et al.*, "Transfer matrix characterization of field-deployed mcfs," in *2020 European Conference on Optical Communications (ECOC)*, (IEEE, 2020), pp. 1–4.
17. E. Deriushkina, J. Schröder, and M. Karlsson, "Dynamic model for coupled-core fibers," J. Lightwave Technol. **42**(23), 8366–8373 (2024).
18. K. Ng, V. Nazarov, S. Kuchinsky, *et al.*, "Analysis of crosstalk in multicore fibers: statistical distributions and analytical expressions," in *Photonics*, vol. 10 (MDPI, 2023), p. 174.
19. M. Koshiba, K. Saitoh, K. Takenaga, *et al.*, "Analytical expression of average power-coupling coefficients for estimating intercore crosstalk in multicore fibers," IEEE Photonics J. **4**(5), 1987–1995 (2012).
20. C. Xia, N. Bai, I. Ozdur, *et al.*, "Supermodes for optical transmission," Opt. Express **19**(17), 16653–16664 (2011).
21. C. Xia, N. Bai, R. Amezcua-Correa, *et al.*, "Supermodes in strongly-coupled multi-core fibers," in *2013 Optical Fiber Communication Conference and Exposition and the National Fiber Optic Engineers Conference (OFC/NFOEC)*, (IEEE, 2013), pp. 1–3.
22. C. Xia, M. A. Eftekhar, R. A. Correa, *et al.*, "Supermodes in coupled multi-core waveguide structures," IEEE J. Sel. Top. Quantum Electron. **22**(2), 196–207 (2015).
23. A. W. Snyder, "Coupled-mode theory for optical fibers," J. Opt. Soc. Am. **62**(11), 1267–1277 (1972).
24. E. Deriushkina, J. Schröder, and M. Karlsson, "Modeling of 3-coupled-core fiber: Comparison between scalar and vector random coupling models," J. Lightwave Technol. **42**(2), 793–801 (2023).
25. M. Karlsson, J. Brentel, and P. A. Andrekson, "Long-term measurement of pmd and polarization drift in installed fibers," J. Lightwave Technol. **18**(7), 941–951 (2000).
26. V. Ribeiro, M. Shi, and A. M. Perego, "Impact of zero-dispersion wavelength fluctuations in a coupled dual-core fiber optical parametric amplifier," J. Lightwave Technol. **41**(19), 6235–6243 (2023).
27. E. Deriushkina, J. Schröder, and M. Karlsson, "Analysis of the scalar and vector random coupling models for a four coupled-core fiber," in *IET Conference Proceedings CP839*, vol. 2023 (IET, 2023), pp. 772–775.
28. M. Raj, V. Ribeiro, G. Bouwmans, *et al.*, "Investigation of nonlinear coupling and parametric interactions in coupled multi-core fibers," in *2025 European Conference on Optical Communications (ECOC)*, (IEEE, 2025), pp. 1–4.
29. R. Ryf, A. Sierra, R.-J. Essiambre, *et al.*, "Coherent 1200-km 6× 6 mimo mode-multiplexed transmission over 3-core microstructured fiber," in *European Conference and Exposition on Optical Communications*, (Optica Publishing Group, 2011), pp. Th–13.
30. H. S. M. Coxeter, "Barycentric coordinates," in *Introduction to Geometry*, (John Wiley and Sons, New York, 1969), pp. 216–221, 2nd ed.
31. A. Edelman and N. R. Rao, "Random matrix theory," Acta Numerica **14**, 233–297 (2005).
32. S. Kotz, N. Balakrishnan, and N. L. Johnson, *Continuous multivariate distributions, Volume 1: Models and applications* (John wiley & sons, 2019).
33. N. L. Johnson, S. Kotz, and N. Balakrishnan, "Beta distributions," Continuous Univariate Distributions **2**, 210–275 (1994).
34. W. H. Beyer, *Crc standard mathematical tables and formulae*, (Boca Raton, 1991).
35. M. Mazur, T. Taunay, T. Geisler, *et al.*, "Measurement of temperature-induced polarization drift and correlation in a 7-core fiber," in *ECOC 2016; 42nd European Conference on Optical Communication*, (VDE, 2016), pp. 1–3.
36. M. Raj, T. Hayashi, P. Andrekson, *et al.*, "Statistical analysis of the temporal dynamics of coupling in strongly coupled multi-core fibers," (2026). https://doi.org/10.5281/zenodo.19019613.